ACS OMEGA

http://pubs.acs.org/journal/acsodf

Article

Role of Interface Structure and Chain Dynamics on the Diverging Glass Transition Behavior of SSBR-SiO_2-PIL Elastomers

Mohammad Abdul Sattar and Archita Patnaik*

Cite This: *ACS Omega* 2020, 5, 21191−21202

Read Online

ACCESS | Metrics & More | Article Recommendations | Supporting Information

ABSTRACT: Intermolecular interactions between the constituents of a polymer nanocomposite at the polymer−particle interface strongly affect the segmental mobility of polymer chains, correlated with their glass transition behavior, and are responsible for the improved dynamical viscoelastic properties. In this work, we emphasized on the evolution of characteristic interfaces and their dynamics in silica (SiO_2 NP)-reinforced, solution-polymerized, styrene butadiene rubber (SSBR) composites, whose relative prevalence varied with the phosphonium ionic liquid (PIL) volume fraction, used as an interfacial modifier. The molecular origins of such interfaces were examined through systematic dielectric spectroscopy, molecular dynamics (MD) simulations, and dynamic-mechanical analyses. The PIL facilitated H-bonding, cation−π, surface−phenyl, and van der Waals interfacial interactions between SSBR and SiO_2 NP, thereby regulating the polymer chain dynamics, orientation, and mean-square displacement. Specifically, the mass density profiles from MD simulations revealed the dynamic gradient of polymer chains in the interfacial region as a function of radial distance from the center of mass of the SiO_2 NP surface. The results showed a structuring effect to result in well-resolved density peaks at specific radial distances with the tangential orientation of styrene monomers in the vicinity of the SiO_2 NP surface. These domino effects highlighted strong interfacial interactions to have an indispensable effect on the viscoelastic performance and thermal motion of SSBR molecular chains, leading to a higher glass transition temperature (T_g) by ∼15 K, validating the experimental data. More importantly, our results gave new insights into the fundamental understanding of the fact that the strength of intermolecular interactions induced by PIL at the polymer−particle interface is the key to control the α-relaxation dynamics and T_g optimization, desired for specific applications.

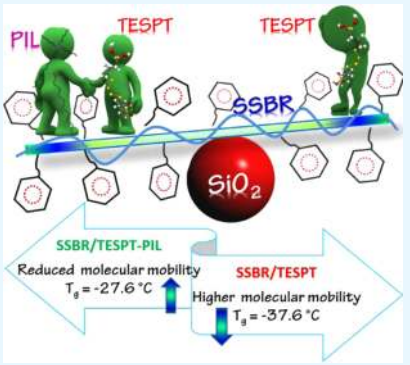

1. INTRODUCTION

The inclusion of filler particles in polymers is essential for enhancing the properties of neat polymers for diverse applications.[1−5] Here, a combination of organic and inorganic materials furnishes composites with benefits from both, giving rise to an additional third phase,[6−8] i.e., the interfacial region that becomes dominant in determining the dynamical−mechanical properties due to different length scales involved. Various factors, such as macromolecular and filler aggregate structures, and the characteristic interfacial interactions have played a major role. However, the two deemed key factors, that have fundamental contributions to the final properties of the nanocomposites are (i) the dispersion of the filler particles in the polymer matrix and (ii) polymer−filler interfacial interactions. Recent experiments and simulations[9−20] have revealed that the thickness and dynamics of the interfacial polymer layer are crucial in enhancing its macroscopic properties. For instance, it was identified that attractive interfacial interactions tend to delay the relaxation dynamics of the polymer chains at the polymer−filler interface. Specifically, nanoparticles (NPs) affect the polymer chain dynamics across the interfacial region and speed up or slow down their dynamics, which changes the glass transition temperature (T_g), correlated with segmental chain dynamics in the neighborhood of the NP surface. Further, the strong tying of polymer chains on the NP surface in a series of dangling tails, loops, and adsorbed segments slows down and broadens the segmental relaxation, accounting for the origin of restricted dynamics. Therefore, the heterogeneity in dynamics depends upon the spatial distance of the segments from the interfaces. Moreover, the presence of a glassy or immobilized (dead polymer layer) interfacial layer has been conjectured (especially in attractive filler−polymer interactions) with slower dynamics, while the weakly attracting and repulsive polymer−filler interactions speed up the relaxation dynamics. Thus, the resulting polymer−filler interface that may impact the structural arrangement and relaxation of the polymer chains under confinement is the subject of extensive research.

Silica (SiO_2) is an essential reinforcing filler for various elastomers.[21−24] However, the silanol groups on the silica

Received: June 18, 2020
Accepted: July 28, 2020
Published: August 13, 2020

Scheme 1. Probable Pathways for the Composite Formation in Absence (a) and Presence (b) of the Phosphonium Ionic Liquid (PIL), Depicting Bonding and Nonbonding Interactions in the Composites

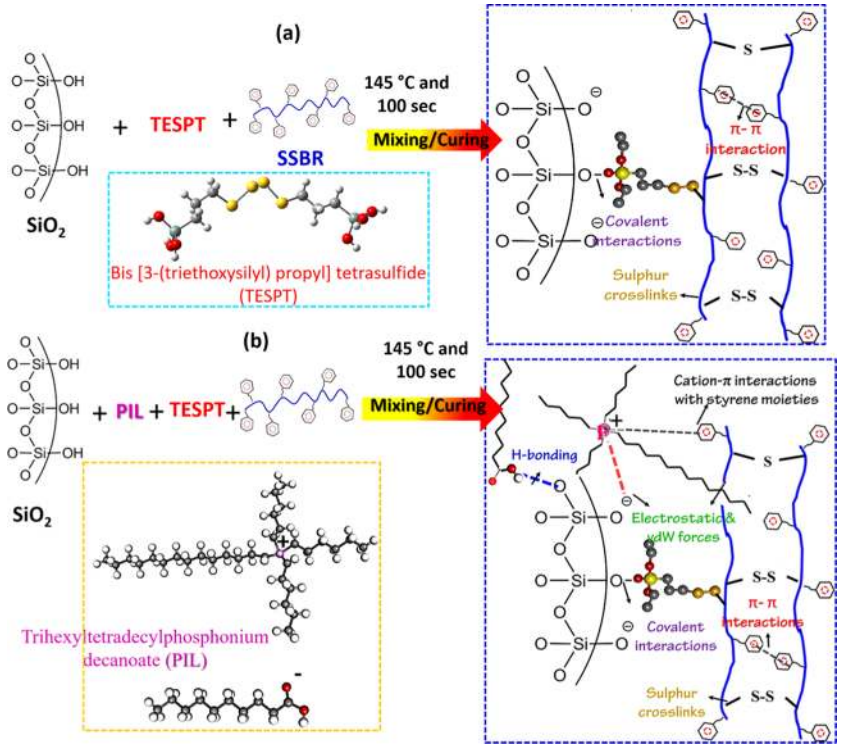

surface induce particle aggregation due to their high surface energy, van der Waals (vdW) forces, and electrostatic interactions. Accordingly, the surface modification of SiO_2 using organic moieties has been employed to improve the material compatibility, interfacial interaction, and dispersion of the filler in a polymer matrix[25−32] through electrostatic, H-bonding, and covalent bonding interactions. For instance, bis[3-(triethoxysilyl) propyl] tetrasulfide (TESPT) has been commonly used in the tire industry to establish a molecular bridge between SiO_2 and SSBR and to cross-link polymer chains during vulcanization. However, the key bottleneck for the implementation of TESPT has been the low reactivity between them, and in this regard, excessive dosage of TESPT has been used to improve the interfacial bonding. To circumvent this, ionic liquids (ILs) as versatile molten salts have been explored with a broad application prospect in the field of green catalysis due to their unique properties such as low melting temperature, high thermal stability, near-zero vapor pressure, and a highly flexible solvating capacity for both polar and nonpolar compounds.[33−35] They have emerged as novel interface modifiers for the surface functionalization of silica with silane coupling agents.[34] Donato et al. introduced alkyl-imidazolium ionic-liquid-modified xerogel silica into melted polymers, yielding improvements in the dispersion and a decrease in filler compactness that increased the nanocomposites' thermal resistance.[36] Covalently bonded 1-(3-trimethoxysilyl propyl)-3-methyl imidazolium chloride-modified silica, compounded with the epoxy polymer, affected the glass transition temperature of the cured hybrid.[37] Studies on IL-driven epoxy-silica systems were performed by Perchacz et al.,[38] illustrating the structure of silica-IL precursors to vary from highly condensed three-dimensional (3D) cagelike to branched ladderlike to cyclic ones. Here, the structure evolution proceeded via H-bonding interactions between the imidazolium ring, the anion, and the growing silicon species, leading to an improvement in thermomechanical properties of the hybrids. In this paper, we propose to use a long aliphatic chain phosphonium-based ionic liquid (trihexyl (tetradecyl) phosphonium decanoate), phosphonium ionic liquid (PIL), as an activator and interface modifier for promoting the interfacial interactions and revealing the molecular origin of the thus-resulting interface structure between SiO_2 NP and solution-polymerized styrene butadiene rubber (SSBR) in the composite. This approach increased the compatibility between the filler and the polymer matrix by exploiting the characteristic nonbonding interactions that significantly improved the thermal and dynamical−mechanical properties. PIL was added during the in situ compounding process, resulting in the composite formation, with no additional processing step or any ex situ filler modification. We examined and parsed the effects imposed by PIL on the structure, glass transition, and segmental dynamics at a scale close to pertinent molecular processes through systematic dielectric spectroscopy, molecular dynamics simulation, and dynamic mechanical analyses. Scheme 1 depicts the details of the composite formation pathways in the presence and absence of PIL.

2. RESULTS AND DISCUSSION

2.1. Segmental Dynamics in SSBR-SiO_2 Composites.

We start our discussion with the influence of PIL on the polymer segmental dynamics of the composites in the vicinity of the filler surface. Figure 1 shows the dielectric response of the composites with different PIL loadings over a broad frequency range using broadband dielectric spectroscopy (BDS). BDS provides intricate data on the polymer chain dynamics and the polymer−filler interface structure[39] along with the reorientation of dipole moments. The reorientation of dipoles occurs through the cooperative motion of the polymer

https://dx.doi.org/10.1021/acsomega.0c02929
ACS Omega 2020, 5, 21191−21202

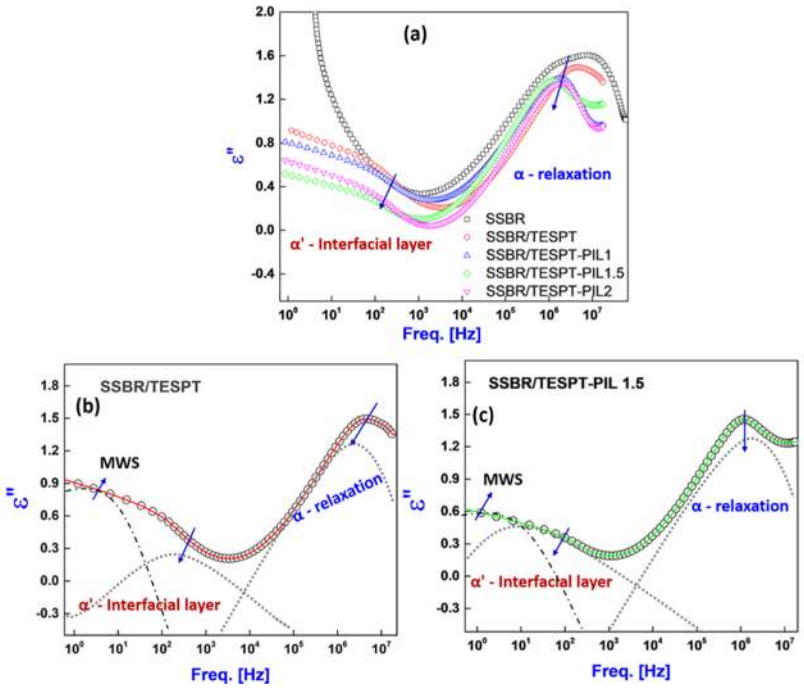

Figure 1. (a) Dielectric loss spectra at a fixed temperature (295 K) for neat SSBR and SSBR-SiO_2 composites with variation in PIL loading. (b, c) Deconvolution of ε'' into varied relaxation processes for (b) SSBR/TESPT and (c) SSBR/TESPT-PIL 1.5 composites. The solid lines are HN fits to the data. The dashed-dotted lines are the contribution of the conductivity and the dotted lines represent the segmental relaxation process (α-relaxation) and interfacial relaxation (α'- relaxation) process.

chains (α-relaxation) or via secondary relaxations (β-relaxation), associated with local motions.[40−45] Here, the α-relaxation, correlated with the dynamic glass transition, can be observed at 295 K due to the segmental motion of SSBR chains. To remove any geometric effects in the samples, the BDS data were normalized with respect to the secondary relaxation process. The spectra clearly show a decrease in the amplitude of the dielectric loss peak arising from the segmental relaxation process in comparison with the neat SSBR. Further, the α-relaxation peak in the composites shifts to lower frequencies at the same isothermal test temperature, indicating restricted polymer chain dynamics near the interfacial region. Such a behavior has been observed for polymer nanocomposites and widely accepted as a new relaxation process.[1,5,8−15,46] The results indicate that the addition of TESPT and increased PIL loading lead to a decrease in the ε'' values due to the replacement of highly polar silanol groups on the silica surface with TESPT and/or PIL molecules. The data in Figure 1a were analyzed to extract quantitative information from the isothermal dielectric measurements using the Havriliak−Negami function (HN function) as

$$\varepsilon^* = \varepsilon_\infty + \frac{\Delta\varepsilon}{\left[1 + (i\omega\tau_{HN})^{\alpha_{HN}}\right]^{\beta_{HN}}} - i\frac{\sigma}{\varepsilon_0\omega^s} \quad (1)$$

Here, $\Delta\varepsilon$ is the dielectric strength, ω is the angular frequency ($\omega = 2\pi f$), τ_{HN} is the relaxation time, the exponents α_{HN} and β_{HN} are shape parameters, and σ is related to the specific dc conductivity. The nonlinear fitting was performed by taking the shape parameters α_{HN} and β_{HN} for the segmental relaxation process (α) in the composites to be equal to those of pristine SSBR and were kept constant during the fit procedure, regardless of the PIL loading. The shape parameters for the interfacial relaxation process (α') were adjusted so as to make it equal to that of the bulklike relaxation and were allowed to vary with PIL concentration. Note that the fitting parameters are tabulated in Table S1, SI. The analyzed data presented in Figure 1a,b at 295 K reveal a relatively low-frequency α'-relaxation, which is attributed to "interfacial relaxation" of the adsorbed layer in the neighborhood of the SiO_2 surface or trapped inside the filler network with restricted dynamics. Interestingly, compared with the SSBR/TESPT composite, an enhanced and broader α'-relaxation in the SSBR/TEPT-PIL 1.5 composite indicates a larger fraction of an interfacially bound polymer, resulting from a synergetic effect of PIL and TESPT in promoting the intermolecular bonding and nonbonding interactions, such as H-bonding, cation−π, and electrostatic interactions. The fitted data in Table S1, SI reveals an appropriately larger dielectric strength $\Delta\varepsilon$ for the PIL-assisted composite along with a lower relaxation time τ_{HN}. Further, in Figure 1, at much lower frequencies, an additional dielectric process is attributed to the Maxwell−Wagner−Sillars (MWS) polarization,[47−49] arising as a result of blocking of charge carriers at internal surfaces of different phases at the interface, having different values of dielectric permittivity and/or conductivity.

2.2. Glass Transition in SSBR-SiO_2 Composites. The T_g of a composite material is strongly reliant on the segmental dynamics of the polymer, which in turn is dependent on intermolecular interactions at the polymer−particle interface. In view of this, dynamic mechanical analysis for all of the composites was done to have a deeper understanding of the reinforcing efficiency of the PIL-incorporated composites. The T_g was determined from the peaks of tan δ curves, related to the segmental mobility of polymer chains,[50] where the filler network could hardly be destroyed. Therefore, the energy dissipation is predominantly due to the friction losses between the polymer chains. Hence, weaker filler−filler interactions improve the internal friction between the polymer chains,

https://dx.doi.org/10.1021/acsomega.0c02929
ACS Omega 2020, 5, 21191−21202

thereby increasing the peak value in the tan δ versus temperature curve.[51] As seen in Figures 2 and S2, SI, the maximum value of tan δ for the SSBR/TESPT-PIL composites is higher than that of SSBR/TESPT and SSBR/PIL composites. Since a SiO_2 particle has abundant silanol groups on its surface even though it has been modified by TESPT, they tend to aggregate and form filler networks in view of low reactivity between SiO_2 and TESPT. On the other hand, in the SSBR/PIL composite (Figure S2, SI), no activation occurs due to the absence of TESPT.Therefore, the relaxation of polymer chains trapped inside the aggregate structure becomes infeasible, leading to a decreased loss factor for SSBR/PIL and SSBR/TESPT composites. In addition, the transmission electron microscopy (TEM) images in the inset of Figure 3a and in Figure S1, SI, show the dispersion of SiO_2 in the SSBR/TESPT composite to be structureless and uneven, containing large SiO_2 aggregates, leading to higher "Payne effect" ($\Delta G'$ = 392), estimated from storage modulus vs % strain measurements. More interestingly, the SSBR/TESPT-PIL 1.5 composite in Figure 3b shows improved and uniformly dispersed SiO_2 particles with few confined polymer fractions with a weaker Payne effect ($\Delta G'$ = 241). The results indicate the enhanced dispersion of the filler in the polymer matrix by PIL. Specifically, the chemical interface formed by the long aliphatic hydrocarbon chain of PIL in the vicinity of SiO_2 particles via nonbonding interactions served as a buffer to prevent the neighboring particles from aggregating.[52,53] This facilitated a larger number of polymer chains to contribute to the loss factor/loss tangent peak in SSBR/TESPT-PIL composites. The molecular-level response of composite materials as a function of temperature and its effect on the storage modulus (E'), loss modulus (E''), and loss factor (tan δ: the energy dissipation potential of the composite) are depicted in Figure 4. Here, the relaxation behavior of the polymer chains due to the inclusion of SiO_2 and PIL cause changes in the segmental (α) and local motion (β) of polymer chains at the polymer−particle interface. Specifically, as shown in Figure 4b, the storage modulus E' values of the SSBR/TESPT-PIL 1.5 composite at low-temperature ranges are much higher compared to those of the SSBR/TESPT composite at similar SiO_2 loading. Interestingly, with increasing temperature, there is no sudden drop in E' for SSBR /TESPT-PIL 1.5; rather, the transitions (T_β and T_α) become wider and shift to higher temperatures. However, the SSBR/TESPT composite registered a sudden drop in E' with lower values. The observed thermal transitions in polymers can be described in terms of free volume changes using the crankshaft mechanism, as shown in Figure 4c. In the crankshaft model, the molecular polymer chain is envisaged as an assembly of mobile segments that have some degree of free movement.[54] As the temperature rises, an increased free volume of the chain segments enhances the molecular motion of polymer chains, resulting in lower material modulus or stiffness.[26,55] The results indicate the presence of PIL to impede the localized and main chain movements of the polymer molecules in the SSBR/TESPT-PIL composite, thereby increasing the storage modulus on account of the involvement of interfacial covalent and nonbonding interactions at the polymer−particle interface. Further, as heating continues, T_g appears when the chains in the amorphous regions begin to coordinate large-scale segmental motion; as shown in Figure 2, T_g is shifted to higher temperatures for all of the composites. However, the T_g curve shifts significantly to a higher temperature (−27.6 °C) in the presence of a silane coupling agent (TESPT) and PIL than in the presence of TESPT alone (−37.6 °C). The nonbonding interactions including ionic cross-links and H-bonding, cation−π, and supramolecular interactions between the adsorbed PIL on SiO_2 and SSBR have restricted the chain mobility, leading to greater stability at elevated temperature.[56] Thus, a synergistic combination of TESPT and PIL aided in reducing the segmental motion of the polymer chains, causing a high-temperature T_g shift.

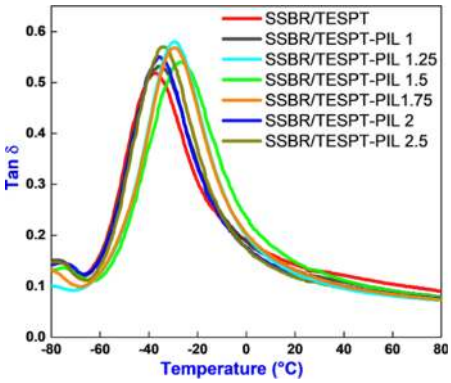

Figure 2. Tan δ vs temperature plot for SSBR-SiO_2 composites at different PIL contents.

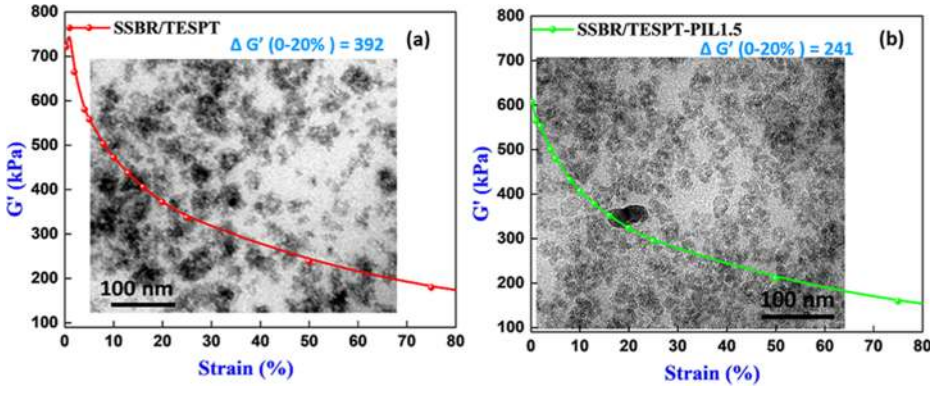

Figure 3. Storage modulus (G')−strain curves for (a) SSBR/TESPT and (b) SSBR/TESPT-PIL 1.5 composites; the insets depict the respective TEM images. $\Delta G'$ is defined as the change in the magnitude of storage modulus between lower strain % (G'_0) and (G'_{20}) higher strain %.

https://dx.doi.org/10.1021/acsomega.0c02929
ACS Omega 2020, 5, 21191−21202

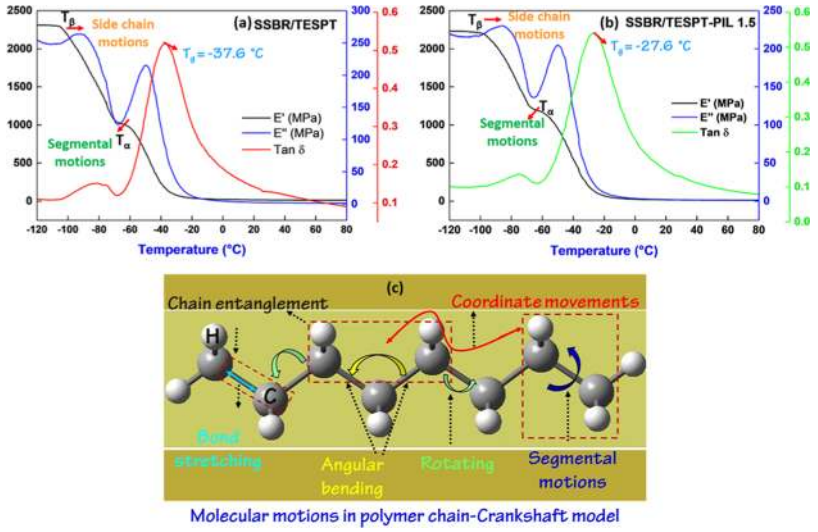

Figure 4. Molecular-level response of composites depicting the storage modulus (E'), loss modulus (E''), and loss factor ($\tan\delta$) as a function of temperature for (a) SSBR/TESPT and (b) SSBR/TESPT-PIL 1.5 composites. (c) Depiction of various molecular motions in the model polymer chain.

Having determined the effect of PIL on glass transition behavior and segmental dynamics at the polymer−particle interface, the following section is devoted to unraveling the molecular mechanisms and nature of interactions underlying the improved interfacial region in composites at a nanoscale. In this context, two composite systems, namely, SSBR/TESPT-PIL (1.5 phr PIL) and SSBR/TESPT, were modeled in addition to neat SSBR using the COMPASS force field.

2.3. Polymer−Filler Interfacial Structure and Dynamics: A Computational Approach. *2.3.1. Building the Model Composites.* The SiO_2 model was trimmed from bulk α-cristobalite in the form of a spherical cluster of radius 10 Å. All of the free unsaturated radicals of the Si atoms in the cluster were first treated by oxygen atoms to mimic the real oxidation process. Further, all of the remaining unsaturated atoms were saturated with H-atoms to satisfy their chemical bonding (Figure 5). To model the functionalized SiO_2 particle, 11 of 104 surface silanol oxygen atoms (grafting ratio: ∼10%) were randomly chosen as the nominee to covalently bond with TESPT, the linker between the SiO_2 particle and the host SSBR matrix. In another case, first, PIL molecules were adsorbed on the surface oxygen atoms of the SiO_2 nanoparticle followed by covalent bond formation with TESPT, as described above. Furthermore, a random copolymer of the SSBR model containing 10 repeat units was built according to the weight content of the structural units present in the commercial SSBR (styrene fraction: 20.8 wt %, 1,2-butadiene fraction: 63.7 wt %). All of the input molecular structures were subjected to energy minimization, following which the minimum energy configuration structures were chosen to construct the amorphous cell (AC) for subsequent MD simulations. Consequently, inside the cubic AC, one SiO_2 NP was embedded in the center surrounded by 100 SSBR chains, of which ∼10 chains were end-functionalized with 3-mercaptopropionic acid[57] under the periodic boundary conditions. Before building the interfacial bonding models, the original AC models were equilibrated for 500 ps at 700 K and 1 atm pressure under NPT ensembles. First, the distance between the unsaturated double bonds in the SSBR matrix and the sulfur atoms of the TESPT-functionalized SiO_2 were monitored and the closest distance was detected. Since real chemical cross-linking[58,59] has been experimentally visualized at a distance smaller than d = 4 Å, the attribution of new bonds in the simulated composite structures in this work followed the same trend. Moreover, a pristine SSBR model was also constructed following the above procedure.

2.3.2. Simulation Details. MD simulations were performed following geometry optimization, where the initial input configurations were first equilibrated by NVT ensemble simulations for 100 ps to release any possible tension and to obtain the stable composite. Consequently, the equilibrated systems were treated under an isothermal−isobaric (NPT) ensemble at 500 K and 1 bar for 1000 ps with a time step of 1 fs until the density of the system remained unchanged. Figure S3, SI, shows the time-evolution density profiles of the nanocomposites, revealing the approach of the pristine bulk polymer regime beyond 800 ps. The molecular interactions initiated by PIL at the interfacial region are shown in Figure S3C, SI. The volumetric and dynamical properties of the composites as a function of temperature were computed from trajectory files. To this end, the above postequilibrated systems were gradually cooled to 80 K by reducing the temperature in a step-wise manner with a temperature interval of 10 K and a cooling rate of 1 K/ps. For structural and dynamic properties, a 500 ps NPT simulation on the output configuration was conducted at 300 K.

2.3.3. Polymer−Filler Intermolecular Interactions and the Interfacial Binding Energy. To study in detail the interface structure and properties, the z-direction distance distribution function between the surface silanol groups and the carbonyl oxygen atoms of the SSBR chain was measured. The probability of finding any specified atom at a distance z from the surface relative to bulk defines the total pair correlation function. Intermolecular interactions such as electrostatic, H-bonding, and van der Waals interactions were considered to be prevailing. A peak value below 3.5 Å indicates covalent and H-bonds, whereas values higher than 3.5 Å indicate van der Waals forces.[14,60,61] Figure 6 shows the radial distribution profiles for SSBR/TESPT-PIL and SSBR/TESPT composites with two intense peaks observed at $r \sim 2.1$ Å and $r \sim 3$ Å, indicating the

https://dx.doi.org/10.1021/acsomega.0c02929
ACS Omega 2020, 5, 21191−21202

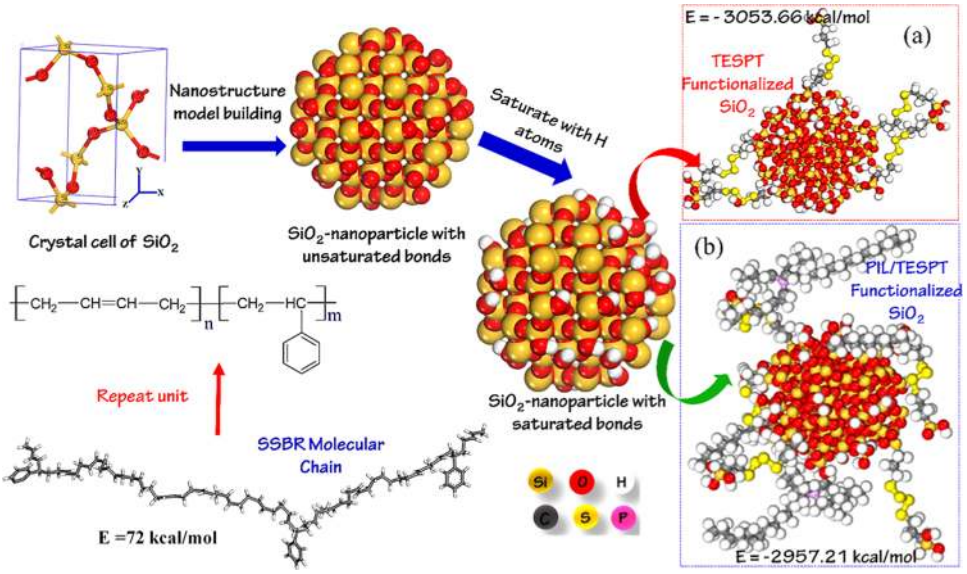

Figure 5. (a, b) Input geometry-optimized molecular structure models of functionalized spherical nano-SiO_2 particles and the SSBR molecular chain.

prevalence of possible electrostatic and H-bonding interactions. In the PIL-based composite, the adsorbed PIL on the silica surface could bring the polymer chains closer via cation−π interactions, thereby modifying the general packing effects near the filler surface. Consequently, more intense peaks for the structural configuration of carbonyl groups of SSBR chains in the SSBR/TESPT-PIL composite are notable. Additionally, a sufficiently intense peak at $r \sim 4.9$ Å, attributed to the effective range of van der Waals interaction, along with observation of weak, long-range interactions at distances $r > 5$ Å implied the interplay of multiple intermolecular forces constituting the interface.

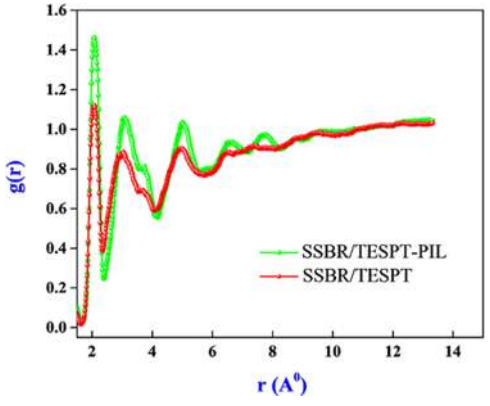

Figure 6. z-direction radial distribution function ($g(r)$) derived for the model composites at 300 K.

The binding energy ($E_{binding}$), defined as the negative of the interaction energy (E_{int}), is a measure of compatibility between the host polymer molecular chain and the nanoparticle that forms new chemical or H-bonds via intermolecular interactions.[59] $E_{int}/E_{binding}$ between the functionalized SiO_2 and SSBR for the model composites can be given as

$$E_{binding} = -E_{inter} = -(E_{total} - E_{SiO_2} - E_{SSBR}) \quad (2)$$

Here, E_{total} is the energy of the SSBR-SiO_2 nanocomposite and E_{SSBR} and E_{SiO_2} are energies of the polymer and silica surface, respectively, implying larger binding energies associated with stronger interactions. Table 1 depicts considerably higher bonded and nonbonded interaction energies for SSBR/TESPT-PIL than the control SSBR/TESPT composite, ascertaining distinct and improved interfacial interactions in the presence of PIL, resulting in a stable interface.

2.3.4. Interfacial Mass Density Profiles and Polymer Chain Orientation. The density distribution of the polymer chains at the SiO_2−polymer interfacial region is a crucial issue as it is directly related to the wetting behavior of the filler.[62−66] Figure 7a shows the radial mass density profiles of the SSBR chains in the model composites as a function of radial distance from the center of mass of the SiO_2 filler surface at 300 K. The results show a structuring effect to result in well-resolved density peaks at specific radial distances beyond which the density profiles reach the bulk. Interestingly, at radial distances larger than 10 Å, high-density regions with respect to the bulk average density (∼1 g/cc) are observed at ∼11−13 and ∼14−16 Å from the surface of the SiO_2 particle with higher intensities. Therefore, the interfacial region can be defined as the entire region from the center of the SiO_2 NP surface to the radial distance where the density reaches the average density of the bulk polymer, as shown in the inset of Figure 7a. We next discuss the impact of the interfacial interactions on the orientation of styrene moieties in the model composites. The global SSBR polymer chain conformation is thus studied. At

Table 1. Energetics in Model SSBR Composites (in kcal/mol) Estimated at 300 K as per eq 2

system	E_{total}	E_{SSBR}	E_{Silica}	E_{int}	E_{bind}	$E_{H\text{-}bond}$	E_{elec}	E_{vdW}
SSBR/TESPT	−3966.4	−733.0	−3053.6	−179.7	179.7	−54.1	−198.3	−163.2
SSBR/TESPT-PIL	−4379.1	−1082.1	−2957.2	−339.8	339.8	−268.5	−438.1	−207.6

https://dx.doi.org/10.1021/acsomega.0c02929
ACS Omega 2020, 5, 21191−21202

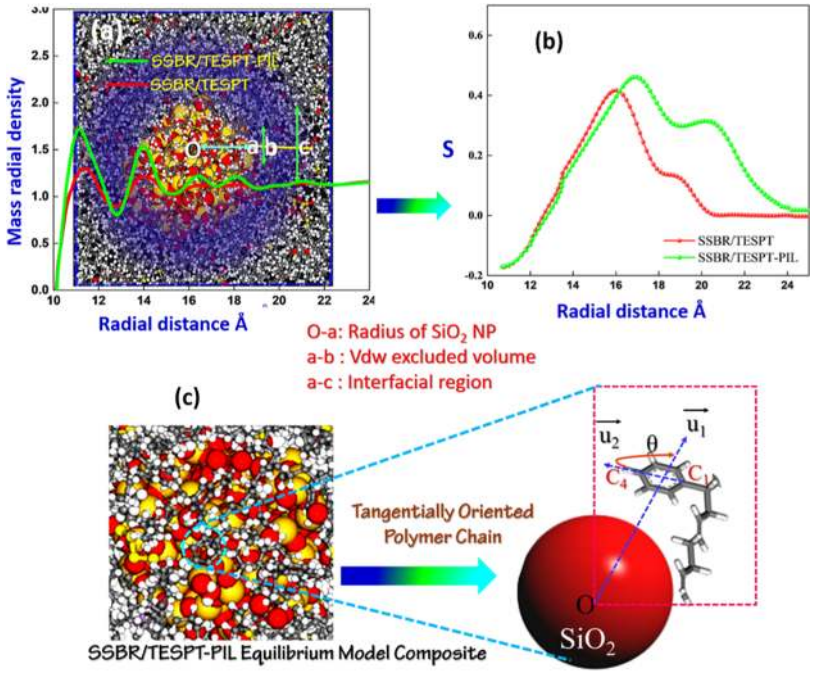

Figure 7. (a) Radial mass density profiles as a function of radial distance from the filler surface. (b) Radial order parameter S of the styrene monomer from the center of the SiO_2 surface. (c) Equilibrium composite model; the inset designates the definition of orientation angle (θ).

the atomistic resolution, the orientation of a single monomer is described by the orientational order parameter (S),[65] which was used to evaluate the spatial orientation of the representing styrene monomer by $S = 1/2\ (3\langle \mathrm{Cos}^2\theta \rangle - 1)$, where θ represents the orientation angle of the monomer segment, characterized by the angle between a fixed monomer vector $\overrightarrow{u_2}$, the surface normal, and the in-plane vector from the phenyl carbon atom C_1 in the direction of C_4 on the SSBR monomer. The unit vector$\overrightarrow{u_1}$ connects the center of mass of the NP to that of the monomer segment. The value of S ranged from −0.2 to 0.5, corresponding to a tangential or radial orientation of the phenyl ring. The random orientation of the phenyl segments was characterized by $S = 0$, and the results are presented in Figure 7b,c showing the definition of θ. The orientation order parameter (S) of the nearest styrene segment to the SiO_2 particle surface is about −0.2 and increases rapidly as the radial distance increases and exhibits a peak at ∼0.4 around 15−19 Å radial distance. Subsequently, S starts to decrease and reaches ∼0, showing the random orientation of the styrene segments. These results indicate the tangential orientation of the phenyl rings in immediate contact with the NP surface, which gradually decreases as the radial distance increases.[62−67] As a matter of fact, the styrene chains in the interfacial region expose mainly their phenyl rings to the NP (Figure 7c). Interestingly, even though the torsion of the styrene segment is only considered a representing torsion of the segment, the orientational order parameter S for the SSBR/TESPT-PIL composite model requires greater separation to reach the average bulk value ($S = 0$) than that in the SSBR/TESPT composite model at the same temperature. We anticipate that the preferential orientation of the phenyl rings near the SiO_2 NP surface could be due to excluded volume effects and surface−phenyl attraction. Accordingly, as shown in Figure 7a, the region ∼11−13 Å from the SiO_2 surface corresponds to the position of the first polymer chain monomer layer along with the second polymer chain monomer layer observed at the density peak corresponding to a radial distance of ∼14−16 Å. However, beyond that layer, S quickly converges to the random average, leading to the random orientation of the phenyl rings. Thus, it is noteworthy to mention that the presence of PIL in the SSBR/TESPT-PIL composite has a larger influence on the segmental alignment of the styrene matrix, i.e., the SSBR/TESPT-PIL model has a larger interfacial region.

2.3.5. Concentration Profiles of the Composite Components. Starting from the respective equilibrium ensembles in Figure 8a,b, in Figure 8c−e, the concentration and density profiles of the polymer (in blue) in immediate contact with the SiO_2 NP (in red) are depicted. It is interesting to note that for the polymer chains to be inclined and concentrated around the SiO_2 NP, however, the likelihood of these chains is higher for the SSBR/TESPT-PIL model composite, as noted in their relative concentrations. To further investigate such an important phenomenon, the density distribution profiles along the z-direction were created and are shown in Figure 8c. Here, the density of polymer chains decreases outward from the central filler particle and converges to the average bulk value. The polymer density in the interfacial region is depicted in white around the spherical SiO_2 NP. As evident from the density maps, a larger number of SSBR molecular chain layers wrap the SiO_2 NP particle relative to the SSBR/TESPT composite model, meaning the existence of a stronger interfacial interaction initiated by PIL,[68,69] which could be the primary reason affecting the distribution of SSBR polymer chain density around the SiO_2 NP.

2.3.6. Simulated Polymer Chain Dynamics and the Glass Transition Temperature (T_g). The mean-square displacement (MSD) and the Einstein relation were used to measure the dynamic properties of the center-of-mass polymer chains, such as their self-diffusion coefficients (D_s), and are given by eqs 3 and 4, respectively.[70]

https://dx.doi.org/10.1021/acsomega.0c02929
ACS Omega 2020, 5, 21191−21202

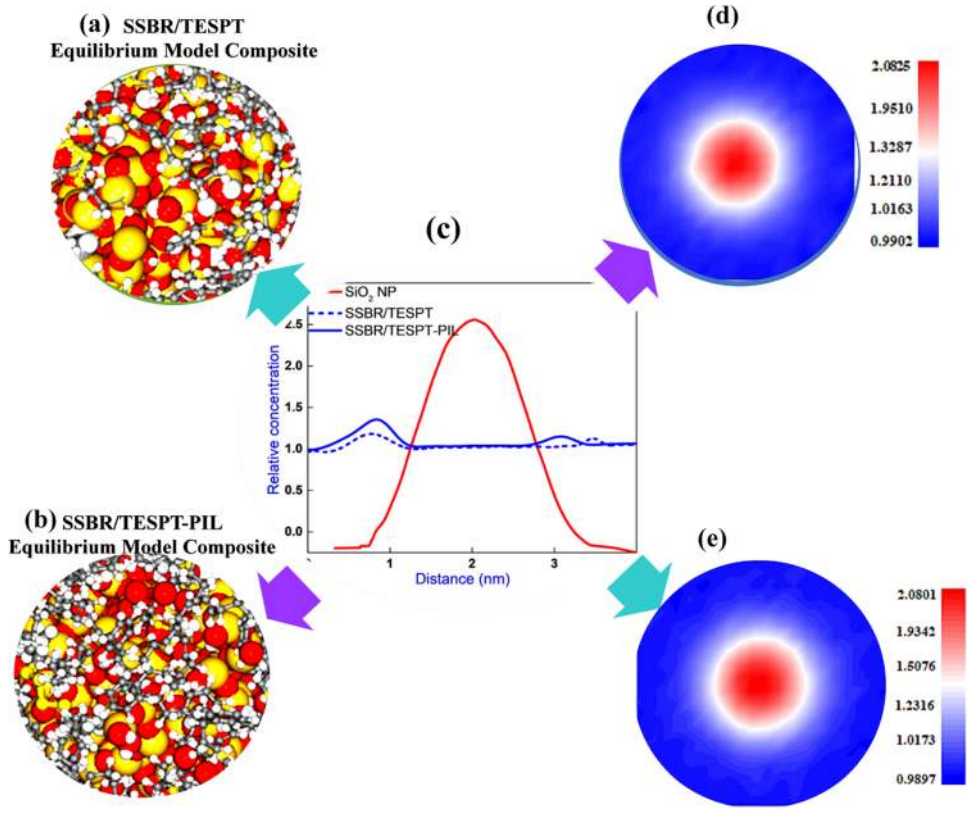

Figure 8. Concentration profile maps of different components in the model nanocomposites derived from the equilibrated ensembles: (a) SSBR/TESPT and (b) SSBR/TESPT-PIL. (c) and (d, e) Corresponding concentration−distance and density contours, respectively, with each color band corresponding to a range of field values.

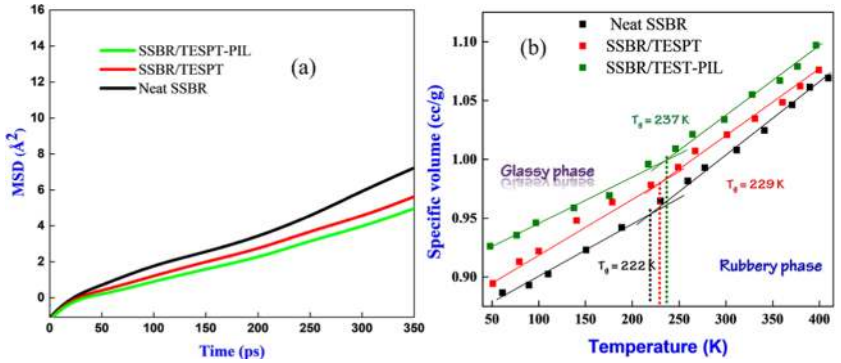

Figure 9. (a) Mean-square displacement of SSBR molecular chains vs time. (b) Change in the specific volume of the amorphous cell with temperature in neat SSBR and the model nanocomposites.

$$\mathrm{MSD} = \langle |r_i(t) - r_i(0)|^2 \rangle \tag{3}$$

$$D_s = \frac{1}{6N} \lim_{t\to\infty} \frac{\mathrm{d}}{\mathrm{d}t} \sum_{i=1}^{N} \langle |r_i(t) - r_i(0)|^2 \rangle \tag{4}$$

where $r_i(t)$ and $r_i(0)$ are position vectors for the ith atom at time "t" and at time $t = 0$, respectively. Calculations were done over all atoms in the polymer chain with N as the number of atoms in the model. The D_s of the polymer chain undergoing random Brownian motion in three dimensions was thus obtained from the limiting slope of the MSD curve, averaged over N atoms as $D_s = \frac{\text{limiting slope}}{6}$. The MSD curves of the two composite models at 300 K are shown in Figure 9a. The greater the D_s from the time curve, the fiercer the chain movement of the polymer and the weaker the thermal stability of the polymer chains.[71,72] Figure 9a reveals the limiting slopes to decrease in both the model composites relative to the neat SSBR polymer model. Further, the SSBR/TESPT-PIL composite exhibited the lowest slope, indicating the restricted mobility of the SSBR polymer chains. It is obvious that the addition of PIL has reduced the strength of the SSBR chain motion via the formation of H-bonds and electrostatic and cation−π interactions between the SiO_2 NP and SSBR, in addition to TESPT cross-links. To explain the influence of the polymer chain dynamics on the specific volume of the model composites, the temperature dependence of specific volume (reciprocal density) was investigated. As a polymer cools down, an abrupt change in its density at T_g brings the system into the glassy state.[73−75] Figure 9b demonstrates the

https://dx.doi.org/10.1021/acsomega.0c02929
ACS Omega 2020, 5, 21191−21202

computed T_g values of the neat polymer and the model composites depicting the glassy and the rubbery phases. An increasing T_g was evident in both the nanocomposite models compared to the pure SSBR host matrix, further denoting a larger T_g for the PIL-based composite. These domino effects highlight the strong interfacial interactions to have an indispensable effect on the thermal motion of SSBR molecular chains, leading to a remarkable increase in the T_g. Collectively, the combination of results indicates that the first interfacial polymer layer the in presence of PIL formed at a distance of ∼1−3 Å from the center of the SiO_2 NP surface with higher polymer chain densities and reduced molecular mobility (tightly bound layer). Similarly, a second polymer nanolayer was formed at a distance of ∼4−6 Å from the NP containing loosely bound polymer chains. The results demonstrate the polymer−filler interactions to be stronger in the SSBR/TESPT-PIL composite, which further reflects in its dynamic mechanical performance (Figures S1 and S6, SI).

3. CONCLUSIONS

The interplay of structure, dynamics, and thermodynamics behind the relative shift in T_g, the roles of binding free energy and intermolecular interactions, the microscopic structural ordering at the interfacial region, and the interfacial interaction energetics have been elucidated via experiments and simulation. The domino effect of phosphonium ionic liquids toward interfacial engineering of the interfacial layer around the filler surface was demonstrated with an indispensable effect on the thermal motion of SSBR molecular chains, leading to a larger T_g. The catalytic effect of PIL as an activator and interface modifier improved the silanization reaction between SiO_2 and TESPT, leading to the creation of a stable interface via H-bonding, cation−π, and electrostatic interactions, in addition to covalent cross-links. The PIL-incorporated composites exhibited overall superior mechanical performance with excellent dynamical behavior. Molecular dynamics simulations revealed the molecular origin of such enhanced dynamical properties of the composites, owing to the existence of a large interfacial layer around the filler surface. The synergistic combination of TESPT and PIL was important in making the stable polymer−filler interface with finer dispersion of filler particles in the host polymer matrix. Furthermore, the novel interface design and the simulation of its structure and dynamics have opened up a new avenue toward the fabrication of high-performance polymer nanocomposites.

4. MATERIALS AND METHODS

4.1. Materials. SSBR (Nipol 1502, styrene fraction: 20.8 wt %, 1,2-butadiene fraction: 63.7 wt %) and polybutadiene rubber were purchased from Laxness Chemical Industry Co., Ltd. Precipitated silica (specific surface area of 193 m^2/g) and Carbon Black N234 were provided by MRF Limited Chennai. Bis[3-(triethoxysilyl) propyl] tetrasulfide (TESPT) was purchased from Evonik. Trihexyl(tetradecyl)phosphonium decanoate (the phosphonium ionic liquid, PIL) was purchased from Sigma-Aldrich. The other chemicals and rubber ingredients were of industrial grade and used as received.

4.2. Preparation of SSBR-SiO_2 Composites. The fundamental compositions of the composites as listed in Table 2 were fabricated according to the processes described in the Supporting Information.

Table 2. Formulation of SSBR-SiO_2 Composites (Unit: phr (Parts per Hundred Rubber))

samples	SSBR	PBD	SiO_2	TESPT	PIL
SSBR/TESPT	70	30	70	7	0
SSBR/TESPT-PIL 1.0	70	30	70	7	1.0
SSBR/TESPT-PIL 1.5	70	30	70	7	1.5
SSBR/TESPT-PIL2.0	70	30	70	7	2.0
SSBR/TESPT-PIL2.5	70	30	70	7	2.5

[a]Other additives*: solution-polymerized styrene butadiene rubber (SSBR), poly butadiene rubber (PBD), *N*-1,3-dimethylbutyl-*N*′-phenyl-*p*-phenylenediamine (6PPD), 2,2,4-trimethyl-1,2-dihydroquinoline (TMQ), *N*-cyclohexyl-2-benzothiazolesulfenamide (CBS), 1,3-diphenylguanidine (DPG), tetrabenzylthiuram disulfide (TBzTD), bis[3-(triethoxysilyl) propyl] tetrasulfide (TESPT), trihexyl tetradecyl phosphonium decanoate (PIL).

4.3. Characterization of SSBR-SiO_2 Composites. The structural morphologies of the nanocomposites were imaged with TEM using the JEM-1010, JEOL instrument at an acceleration voltage of 80 kV. For imaging, thin slices of the sample of thickness ∼120 nm were obtained by cryomicrotoming at −120 °C using a Leica EM FC6 instrument and were anchored on carbon-coated copper grids.

4.4. Broadband Dielectric Spectroscopy (BDS). The polymer chain dynamics in the composites was studied by BDS using an α high-resolution dielectric analyzer (Novocontrol Technologies GmbH, Hundsangen, Germany). The complex permittivity $\varepsilon^*(\omega) = \varepsilon'(\omega) - i\varepsilon''(\omega)$ was measured by carrying out isothermal frequency sweeps over a wide frequency range of $10^{-1} < f$ (Hz) $< 10^7$ (where $f = \omega/2\pi$ is the frequency of the applied electric field and ω is the angular frequency). The circular-shaped samples were placed between two parallel gold-plated electrodes in the dielectric cell for measuring the permittivity. The sample temperature was regulated using a Quattro temperature controller with nitrogen gas flow providing a temperature stability better than ±0.1 K during every single frequency sweep.

Dynamic mechanical properties of the vulcanizates were determined using a METRAVIB 50N (France) dynamic mechanical thermal analyzer in tension mode. Temperature sweep experiments were carried out at 1 Hz frequency and 0.1% dynamic strain. The scanning temperature range was from −100 to +100 °C at a ramp rate of 3 °C/min.

4.5. Molecular Dynamics Simulations. Molecular dynamics simulations were performed using Material Studio 5.0 (Accelrys Inc., San Diego, CA) simulation package with the COMPASS force field. A velocity Verlet algorithm with a time integration step of 1 fs was used for atom motion equations. The nonbonded vdW (van der Waals) interactions were truncated at 12.5 Å. Atom-based and Ewald summation methods were used for vdW and Coulomb interactions, respectively. In addition, a Nosé−Hoover thermostat and a Berendsen barostat were used to control the temperature and pressure in all NPT (isothermal−isobaric ensemble) simulations, respectively.

■ ASSOCIATED CONTENT

Supporting Information

The Supporting Information is available free of charge at https://pubs.acs.org/doi/10.1021/acsomega.0c02929.

Mechanical properties of SSBR-SiO_2 composites; their storage modulus, stress−strain curves, and rheology,

https://dx.doi.org/10.1021/acsomega.0c02929
ACS Omega 2020, 5, 21191−21202

including the methodology for composite formation (PDF)

AUTHOR INFORMATION

Corresponding Author

Archita Patnaik − *Colloid and Interface Chemistry Laboratory, Department of Chemistry, Indian Institute of Technology Madras, Chennai 600036, India;* orcid.org/0000-0002-0754-7055; Phone: 044-2257-4217; Email: archita59@yahoo.com; Fax: 044-2257-4202

Author

Mohammad Abdul Sattar − *Colloid and Interface Chemistry Laboratory, Department of Chemistry, Indian Institute of Technology Madras, Chennai 600036, India; R&D Centre, MRF Limited, Chennai 600019, India;* orcid.org/0000-0002-4267-6805

Complete contact information is available at: https://pubs.acs.org/10.1021/acsomega.0c02929

Notes

The authors declare no competing financial interest.

ACKNOWLEDGMENTS

The authors thank the Department of Physics, IIT Madras for making available the Broad band Dielectric Spectroscopy facility. Financial support from MRF Ltd. Chennai, India, is gratefully acknowledged.

REFERENCES

(1) Lin, Y.; Hu, S.; Wu, G. Structure, Dynamics, and Mechanical Properties of Polyimide-Grafted Silica Nanocomposites. *J. Phys. Chem. C* **2019**, *123*, 6616−6626.

(2) Vogt, B. D. Mechanical and Viscoelastic Properties of Confined Amorphous Polymers. *J. Polym. Sci., Part B: Polym. Phys.* **2018**, *56*, 9−30.

(3) Liu, J.; Min, B.; Wang, Z.; Teng, J.; Sun, Xi.; Shaofan, Li.; Shuzhou, Li. Influence of functionalized core-shell structure on the thermodynamic and shape memory properties of nanocomposites. *Nanoscale* **2020**, *12*, 3205−3219.

(4) Teng, J.; Wang, Z.; Liu, J.; Sun, Xi. Effect of dynamic vulcanization system on the thermodynamics and shape memory properties of TPI/HDPE hybrid shape memory polymers. *Eur. Polym. J.* **2020**, *132*, No. 109707.

(5) Klonos, P.; Pissis, P.; Kyritsis, A. Effects of Hydration/Dehydration on Interfacial Polymer Fraction and Dynamics in Nanocomposites Based on Metal-Oxides and Physically Adsorbed Polymer. *J. Phys. Chem. C* **2017**, *121*, 19428−19441.

(6) Liu, J.; Wang, Z.; Li, S.; Tenga, J.; Mina, B. Development of functionalized core-shell nanohybrids/synthetic rubber nanocomposites with enhanced performance. *Soft Matter* **2019**, *15*, 8338−835.

(7) Marjan, A. K.; Nitin, M.; Jiahua, Z. A review on the role of interface in mechanical, thermal, and electrical properties of polymer composites. *Adv. Compos. Hybrid Mater.* **2018**, 415−439.

(8) Cheng, S.; Carroll, B.; Bocharova, V.; Carrillo, J.-M.; Sumpter, B. G.; Sokolov, A. P. Focus: Structure and dynamics of the interfacial layer in polymer nanocomposites with attractive interactions. *J. Chem. Phys.* **2017**, *146*, No. 203201.

(9) Torres, J. M.; Stafford, C. M.; Vogt, B. D. Elastic Modulus of Amorphous Polymer Thin Films: Relationship to the Glass Transition Temperature. *ACS Nano* **2009**, *3*, 2677−2685.

(10) Khatiwada, B. K.; Blum, F. D. Tightly Bound PMMA on Silica Has Reduced Heat Capacities. *Langmuir* **2019**, *35*, 11482−11490.

(11) Genix, A. C.; Baeza, G. P.; Oberdisse, J. Recent advances in structural and dynamical properties of simplified industrial nanocomposites. *Eur. Polym. J.* **2016**, *85*, 605−619.

(12) Sahraei, A. A.; Mokarizadeh, A. H.; George, D.; Rodrigue, D.; Baniassadiac, M.; Foroutan, M. Insights into interphase thickness characterization for graphene/epoxy nanocomposites: a molecular dynamics simulation. *Phys. Chem. Chem. Phys* **2019**, *21*, 19890−19903.

(13) Hetayothin, B.; Cabaniss, R. A.; Blum, F. D. Does Plasticizer Penetrate Tightly Bound Polymer in Adsorbed Poly (vinyl acetate) on Silica. *Macromolecules* **2017**, *50*, 2092−2102.

(14) Mortazavian, H.; Fennell, C. J.; Blum, F. D. Structure of the Interfacial Region in Adsorbed Poly (vinyl acetate) on Silica. *Macromolecules* **2016**, *49*, 298−307.

(15) Klonos, P. A.; Nosach, L. V.; Voronin, E. F.; Pakhlov, E. M.; Kyritsis, A.; Pissis, P. Glass Transition and Molecular Dynamics in Core-Shell-Type Nanocomposites Based on Fumed Silica and Polysiloxanes: Comparison between Poly(dimethylsiloxane) and Poly(ethylhydrosiloxane). *J. Phys. Chem. C* **2019**, *123*, 28427−28436.

(16) Wang, C.; Deitrick, K.; Seo, J.; Cheng, Z.; Zacharia, N. S.; Weiss, R. A.; Vogt, B. D. Manipulating the Mechanical Response of Hydrophobically Cross-Linked Hydrogels with Ionic Associations. *Macromolecules.* **2019**, *52*, 6055−6067.

(17) Chakraborty, S.; Lim, C. H.; Jun, Y. Achieving an Optimal T_g Change by Elucidating the Polymer-Nanoparticle Interface: A Molecular Dynamics Simulation Study of the Poly (vinyl alcohol)-Silica Nanocomposite System. *J. Phys. Chem. C* **2019**, *123*, 23995−24006.

(18) Nguyen, H. K.; Inutsuka, M.; Kawaguchi, D.; Tanaka, K. Direct Observation of Conformational Relaxation of Polymer Chains at Surfaces. *ACS Macro Lett.* **2018**, *7*, 1198−1202.

(19) Nguyen, H. K.; Sugimoto, S.; Konomi, A.; Inutsuka, M.; Kawaguchi, D.; Tanaka, K. Dynamics Gradient of Polymer Chains near a Solid Interface. *ACS Macro Lett* **2019**, *8*, 1006−1011.

(20) Kempfer, K.; Devemy, J.; Dequidt, A.; Couty, M.; Malfreyt, P. Atomistic Descriptions of the cis-1,4-Polybutadiene/Silica Interfaces. *ACS Appl. Polym. Mater* **2019**, *1*, 969−981.

(21) Stöckelhuber, K. W.; Svistkov, A. S.; Pelevin, A. G.; Heinrich, G. Impact of Filler Surface Modification on Large Scale Mechanics of Styrene Butadiene/Silica Rubber Composites. *Macromolecules* **2011**, *44*, 4366−4381.

(22) Baeza, G. P.; Genix, A.-C.; Degrandcourt, C.; Petitjean, L.; Gummel, J.; Schweins, R.; Couty, M.; Oberdisse, J. Effect of Grafting on Rheology and Structure of a Simplified Industrial Nanocomposite Silica/SBR. *Macromolecules* **2013**, *46*, 6621−6633.

(23) Gui, Y.; Zheng, J.; Ye, X.; Han, D.; Xi, M.; Zhang, L. Preparation and performance of silica/SBR masterbatches with high silica loading by latex compounding method. *Composites, Part B* **2016**, *85*, 130−139.

(24) Wolff, S. Chemical Aspects of Rubber Reinforcement by Fillers. *Rubber Chem. Technol.* **1996**, *69*, 325−346.

(25) Araujo-Morera, J.; Hernandez, M.; Verdejo, R.; Lopez-Manchado, M. A. Giving a second opportunity to tire waste: An alternative path for the development of sustainable self-healing styrene-butadiene rubber compounds overcoming the magic triangle of tires. *Polymers* **2019**, *11*, No. 2122.

(26) Zou, Y.; Sun, Y.; He, J.; Tang, Z.; Zhu, L.; Luo, Y.; Liu, F. Enhancing mechanical properties of styrene-butadiene rubber/silica nanocomposites by in situ interfacial modification with a novel rare-earth complex. *Composites, Part A* **2016**, *87*, 297−309.

(27) Pattanawanidchai, S.; Loykulnant, S.; Sae-oui, P.; Maneevas, N.; Sirisinha, C. Development of eco-friendly coupling agent for precipitated Silica Filled Natural Rubber Compounds. *Polym. Test.* **2014**, *34*, 58−63.

(28) Nah, C.; Huh, M.-Y.; Rhee, J. M.; Yoon, T.-H. Plasma surface modification of silica and its effect on properties of styrene-butadiene rubber compound. *Polym. Int.* **2002**, *51*, 510−518.

(29) Sattar, M. A.; Nair, A. S.; Xavier, P. J.; Patnaik, A. Natural rubber-SiO_2 nanohybrids: interface structures and dynamics. *Soft Matter* **2019**, *15*, 2826−2837.
(30) Sattar, M. A.; Gangadharan, S.; Patnaik, A. Design of Dual Hybrid Network Natural Rubber-SiO_2 Elastomers with Tailored Mechanical and Self-Healing Properties. *ACS Omega* **2019**, *4*, 10939−10949.
(31) Zheng, J.; Han, D.; Zhao, S.; Ye, X.; Wang, Y.; Wu, Y.; Dong, D.; Liu, J.; Wu, X.; Zhang, L. Constructing a Multiple Covalent Interface and Isolating a Dispersed Structure in Silica/Rubber Nanocomposites with Excellent Dynamic Performance. *ACS Appl. Mater. Interfaces* **2018**, *10*, 19922−19931.
(32) Tang, Z.; Huang, J.; Wu, X.; Guo, B.; Zhang, L.; Liu, F. Interface Engineering towards Promoting Silanization by Ionic Liquid for High-Performance Rubber/Silica Composites. *Ind. Eng. Chem. Res.* **2015**, *54*, 10747−10756.
(33) Livi, S.; Chardin, C.; Lins, L.; Halawani, N.; Pruvost, S.; Duchet-Rumeau, J.; Gerard, J. F.; Baudoux, J. From Ionic Liquid Epoxy Monomer to Tunable Epoxy-Amine Network: Reaction Mechanism and Final Properties. *ACS Sustainable Chem. Eng.* **2019**, *7*, 3602−3613.
(34) Livi, S.; Giannelis, E. P. An improved process for the surface modification of SiO_2 nanoparticles. *Green Chem.* **2012**, *14*, 3013−3015.
(35) Castillo, M. R.; Fraile, J. M.; Mayoral, J. A. Structure and Dynamics of 1-Butyl-3-methylimidazolium Hexafluorophosphate Phases on Silica and Laponite Clay: From Liquid to Solid Behavior. *Langmuir* **2012**, *28*, 11364−11375.
(36) Donato, R. K.; Benvegnu, M. A.; Furlan, L. G.; Mauler, R. S.; Schrekker, H. S. Imidazolium salts as liquid coupling agents for the preparation of polypropylene-silica composites. *J. Appl. Polym. Sci.* **2010**, *116*, 304−307.
(37) Carvalho, A. P. A.; Soares, B. G.; Livi, S. Organically modified silica (ORMOSIL) bearing imidazolium-based ionic liquid prepared by hydrolysis/co-condensation of silane precursors: Synthesis, characterization and use in epoxy networks. *Eur. Polym. J.* **2016**, *83*, 311−322.
(38) Perchacz, M.; Donato, R. K.; Seixas, L.; Zhigunov, A.; Serkis-rodzen, M.; Benes, H.; et al. Ionic Liquid-Silica Precursors via Solvent-Free Sol-Gel Process and Their Application in Epoxy-Amine Network: A Theoretical/Experimental Study. *ACS Appl. Mater. Interfaces* **2017**, *9*, 16474−16487.
(39) Kremer, F.; Schönhals, A. *Broadband Dielectric Spectroscopy*; Springer: New York, 2003; p 721.
(40) Zhang, Z.-B.; Fujiki, M.; Tang, H.-Z.; Motonaga, M.; Torimitsu, K. The First High Molecular Weight Poly(N-alkyl-3,6-carbazole)s. *Macromolecules* **2002**, *35*, 1988−1990.
(41) Sanchez, V.; Hernandez, M.; Tiberio, A. E.; l Verdejo, R.; Lopez-Manchado, M. A. In-situ cure monitoring of epoxy/graphene nanocomposites by several spectroscopic techniques. *Polym. Test.* **2019**, *80*, No. 106114.
(42) Janik, P.; Paluch, M.; Ziolo, J.; Sulkowski, W.; Nikiel, L. Low-frequency dielectric relaxation in rubber. *Phys. Rev. E* **2001**, *64*, No. 042502.
(43) Meier, J. G.; Mani, J. W.; Klüppel, M. Analysis of carbon black networking in elastomers by dielectric spectroscopy. *Phys. Rev. B* **2007**, *75*, No. 054202.
(44) Füllbrandt, M.; Purohit, P. J.; Schönhals, A. Combined FTIR and Dielectric Investigation of Poly (vinyl acetate) Adsorbed on Silica Particles. *Macromolecules* **2013**, *46*, 4626−4632.
(45) Utrera-Barrios, S.; Hernandez, M.; Verdejo, R.; Lopez-Manchado, M. A. Design of Rubber Composites with Autonomous Self-Healing Capability. *ACS Omega* **2020**, *5*, 1902−1910.
(46) Rathi, A.; Hernandez, M.; Garcia, S. J.; Dierkes, W. K.; Noordermeer, M.; Bergmann, C.; Trimbach, J.; Blume, A. Identifying the Effect of Aromatic Oil on the Individual Component Dynamics of S-SBR/BR Blends by Broadband Dielectric Spectroscopy. *J. Polym. Sci., Part B: Polym. Phys.* **2018**, *56*, 842−854.
(47) Carroll, B.; Cheng, S.; Sokolov, A. P. Analyzing the Interfacial Layer Properties in Polymer Nanocomposites by Broadband Dielectric Spectroscopy. *Macromolecules* **2017**, *50*, 6149−6163.
(48) Holt, A. P.; Sangoro, J. R.; Wang, Y.; Agapov, A. L.; Sokolov, A. P. Chain and Segmental Dynamics of Poly(2-vinylpyridine) Nanocomposites. *Macromolecules* **2013**, *46*, 4168−4173.
(49) Holt, A. P.; Griffin, P. J.; Bocharova, V.; Agapov, A. L.; Imel, A. E.; Dadmun, M. D.; Sangoro, J. R.; Sokolov, A. P. Dynamics at the Polymer/Nanoparticle Interface in Poly(2-vinylpyridine)/Silica Nanocomposites. *Macromolecules* **2014**, *47*, 1837−1843.
(50) Huda, M. S.; Drzal, L. T.; Mohanty, A. K.; Misra, M. Effect of fiber surface-treatments on the properties of laminated biocomposites from poly(lactic acid) (PLA) and kenaf fibers. *Compos. Sci. Technol.* **2008**, *68*, 424−432.
(51) Robertson, C. G.; Lin, C. J.; Rackaitis, M.; Roland, C. M. Influence of Particle Size and Polymer-Filler Coupling on Viscoelastic Glass Transition of Particle-Reinforced Polymers. *Macromolecules* **2008**, *41*, 2727−2731.
(52) Wang, M.; Mahmud, K.; Murphy, L.; Patterson, W. Carbon-silica dual phase filler, a new generation reinforcing agent for rubber. Part I characterization. *Kautsch. Gummi Kunstst.* **1998**, *51*, 348−360.
(53) Rao; Pochan, J. M. Mechanics of Polymer−Clay Nanocomposites. *Macromolecules* **2007**, *40*, 290−296.
(54) Flory, P. J. *Principles of Polymer Chemistry*; Cornell University Press, 1953.
(55) Jayanarayanan, K.; Rasana, N.; Mishra, R. K. Dynamic Mechanical Thermal Analysis of Polymer Nanocomposites. *Therm. Rheol. Meas. Tech. Nanomater. Charact.* **2017**, 123−157.
(56) Stein, S.; Mordvinkin, A.; Voit, B.; Komber, H.; Saalwächter, K.; Böhme, F. Self-healing and reprocessable bromo butylrubber based on combined ionic cluster formation and hydrogen bonding. *Polym. Chem.* **2020**, *11*, 1188−1197.
(57) Luo, Y.; Liu, H.; Xiang, B.; Chen, Xi.; Yang, W.; Luo, Z. Temperature dependence of the interfacial bonding characteristics of silica/styrene butadiene rubber composites: a molecular dynamics simulation study. *RSC Adv.* **2019**, *9*, 40062−40071.
(58) Song, M.; Zhao, X.; Li, Y.; Hu, S.; Zhang, L.; Wu, S. Molecular dynamics simulations and microscopic analysis of the damping performance of hindered phenol AO-60/nitrile-butadiene rubber composites. *RSC Adv.* **2014**, *4*, 6719−6729.
(59) Luo, Y.; Qu, L.; Su, H.; Chan, T. W.; Wu, S. Effect of chemical structure of elastomer on filler dispersion and interactions in silica/solution-polymerized styrene butadiene rubber composites through molecular dynamics simulation. *RSC Adv.* **2016**, *6*, 14643−14650.
(60) Wang, Y.; Li, X.; Wei, Q.; Yang, M.; Wei, S. Study on the Mechanical Properties of Three-Dimensional Directly Binding Hydroxyapatite Powder. *Cell Biochem. Biophys.* **2015**, *72*, 289−295.
(61) Wei, Q.; Zhang, Y.; Wang, Y.; Yang, M. A molecular dynamic simulation method to elucidate the interaction mechanism of nano-SiO_2 in polymer blends. *J. Mater. Sci.* **2017**, 12889−12901.
(62) Ndoro, T. V. M.; Voyiatzis, E.; Ghanbari, A.; Theodorou, D. N.; Böhm, M. C.; Müller-Plathe, F. Interface of Grafted and Ungrafted Silica Nanoparticles with a Polystyrene Matrix: Atomistic Molecular Dynamics Simulations. *Macromolecules* **2011**, *44*, 2316−2327.
(63) Ndoro, T. V. M.; Böhm, M. C.; Müller-Plathe, F. Interface and Interphase Dynamics of Polystyrene Chains near Grafted and Ungrafted Silica Nanoparticles. *Macromolecules* **2012**, *45*, 171−179.
(64) Ghanbari, A.; Ndoro, T. V. M.; Leroy, F.; Rahimi, M.; Böhm, M. C.; Müller-Plathe, F. Interphase Structure in Silica-Polystyrene Nanocomposites: A Coarse-Grained Molecular Dynamics Study. *Macromolecules* **2012**, *45*, 572−584.
(65) Wang, Z.; Lv, Q.; Chen, S.; Li, C.; Sun, S.; Hu, S. Effect of Interfacial Bonding on Interphase Properties in SiO_2/Epoxy Nanocomposite: A Molecular Dynamics Simulation Study. *ACS Appl. Mater. Interfaces* **2016**, *8*, 7499−7508.
(66) Chen, T.; Qian, H.-J.; Zhu, Y.-L.; Lu, Z.-Y. Structure and Dynamics Properties at Interphase Region in the Composite of

https://dx.doi.org/10.1021/acsomega.0c02929
ACS Omega 2020, 5, 21191−21202

Polystyrene and Cross-Linked Polystyrene Soft Nanoparticle. *Macromolecules* **2015**, *48*, 2751−2760.
(67) Zuo, B.; Inutsuka, M.; Kawaguchi, D.; Wang, Xi.; Tanaka, K. Conformational Relaxation of Poly(styrene-co-butadiene) Chains at Substrate Interface in Spin-Coated and Solvent-Cast Films. *Macromolecules* **2018**, *51*, 2180−2186.
(68) Wei, Q.; Wang, Y.; Wang, S.; Zhang, Y.; Chen, X. Investigating the properties and interaction mechanism of nano-silica in polyvinyl alcohol/polyacrylamide blends at an atomic level. *J. Mech. Behav. Biomed. Mater.* **2017**, *75*, 529−537.
(69) Tang, C.; Li, X.; Li, Z.; Hao, J. Interfacial Hydrogen Bonds and Their Influence Mechanism on Increasing the Thermal Stability of Nano-SiO_2-Modified Meta-Aramid Fibers. *Polymers* **2017**, *9*, No. 504.
(70) Teraoka, I. *Polymer Solutions: An Introduction to Physical Properties*; Wiley-Interscience: New York, 2002; p 176.
(71) Wei, Q.; Wang, Y.; Zhang, Y.; Chen, X. Aggregation Behavior of Nano-Silica in Polyvinyl Alcohol/Polyacrylamide Hydrogels Based on Dissipative Particle Dynamics. *Polymers* **2017**, *9*, No. 611.
(72) Saha, S.; Bhowmick, A. K. An Insight into molecular structure and properties of flexible amorphous polymers: A molecular dynamics simulation approach. *J. Appl. Polym. Sci.* **2019**, *136*, No. 47457.
(73) Ryu, M. S.; Kim, H. G.; Kim, H. Y.; Min, K. S.; Kim, H. J.; Lee, H. M. Prediction of the glass transition temperature and design of phase diagrams of butadiene rubber and styrene-butadiene rubber via molecular dynamics simulations. *Phys. Chem. Chem. Phys.* **2017**, *19*, 16498−16506.
(74) Wang, Y.-h.; Wang, W.-h.; Zhang, Z.; Xu, L.; Li, P. Study of the glass transition temperature and the mechanical properties of PET/modified silica nanocomposite by molecular dynamics simulation. *Eur. Polym. J.* **2016**, *75*, 36−45.
(75) Yang, Q.; Chen, X.; He, Z.; Lan, F.; Liu, H. The glass transition temperature measurements of polyethylene: determined by using molecular dynamic method. *RSC Adv.* **2016**, *6*, 12053−12060.

https://dx.doi.org/10.1021/acsomega.0c02929
ACS Omega 2020, 5, 21191−21202